Int. J. Multiphase Flow Vol. 6, pp. 523–551
Pergamon/Elsevier, 1980. Printed in Great Britain

MULTIVARIATE HYDRODYNAMIC ANALYSIS OF BOILING CHANNEL FLOW STABILITY FROM INHERENT NOISE MEASUREMENTS

T. M. ROMBERG
Engineering Research Division, Australian Atomic Energy Commission, Research Establishment, Lucas Heights, NSW 2234, Australia

and

N. W. REES
University of NSW, Kensington, NSW 2033, Australia

(*Received* 20 *November* 1979; *in revised form* 8 *June* 1980)

Abstract—Perturbations in the inlet flow, temperature, channel power, pressure drop and exit void fraction were monitored on a test channel for a range of power levels up to flow stability threshold. Multivariate spectral analysis methods are used to determine the significant frequency response relationships between the measured variables, and the significant cross-spectral density estimates are compared with those obtained from a distributed frequency domain model whose subcooled boiling, two-phase slip and friction correlations are optimised using a special parameter estimation procedure. The optimised model gives the physical mechanisms (perturbed pressure drop components) which tend to drive the channel unstable. The spectral analysis and modelling techniques are generally applicable to performance and diagnostic studies in commercial heat transfer plant where traditional methods of superimposing test signals are impractical during normal operation.

1. INTRODUCTION

The performance and reliability of nuclear and conventional steam generators, process heat exchangers, thermo-syphon reboilers and other two-phase heat transfer equipment are dependent on the steady flow of coolant through their component heated channels. Under certain operating conditions (coolant pressures, temperatures, flow rates, heat fluxes etc.), a variety of fundamental and higher mode coolant flow instabilities can occur which may not be detected until some catastrophic failure (e.g. boiler tube burnout, corrosion or rupture) terminates normal operation. Prior to the onset of coolant flow oscillations, the plant variables (flow rate, pressures, temperatures, etc.) fluctuate about some nominal steady state operating condition, and there is an incentive to utilise this "hydrodynamic noise" for performance and diagnostic testing, particularly in commercial plant where traditional methods of superimposing test signals are impractical during normal operation.

Although there have been numerous flow stability investigations in recent years covering a wide range of experimental and commercial applications (see reviews by Bergles 1972, Boure *et al.* 1973), very few have attempted to exploit the inherent hydrodynamic noise for performance and diagnostic assessment of the plant behaviour. Notable exceptions are the hydrodynamic noise studies on the Halden reactor (Eurola 1963), the prototype SGHWR† (Gall 1973) and Japanese BWRs† (Fukunishi 1977). The Halden reactor studies investigated a number of single input single output (SISO) relationships, and concluded that inherent noise techniques "are a very useful supplementary tool to other experimental techniques in the study of system dynamics, but are not as powerful as external perturbation methods in certain areas" (Uhrig 1970, p. 430). Spigt (1966) also observed from his own investigations that inherent noise methods warrant further development and evaluation work. The SGHWR study (Gall 1973) computed the autocorrelation and power spectral density functions of the channel inlet flowmeter noise, and compared these results with the impulse response functions of a space-time finite difference hydrodynamics model by assuming the reactor was a second order autoregressive process (Jenkins & Watts 1968). A similar investigation has been reported more

†SGHWR—Steam Generating Heavy Water Reactor; BWR—Boiling Water Reactor.

recently by Rakopoulos *et al.* (1978). The Japanese BWR studies (Fukunishi 1977) monitored seven plant variables, and used multivariate spectral analysis methods to assess the degree of interaction (coherence) between variables. Some empirical multivariable autoregressive modelling has also been attempted (Fukunishi & Kiyokawa 1976). However, despite the initial optimism regarding the potential of inherent noise techniques, most hydrodynamic investigations have used external perturbations, usually sinusoids, possibly for practical and conservative reasons.

The principal aim of this paper is to show that inherent noise analysis techniques, when used in a complementary interactive manner with a distributed theoretical model, give significantly more information about the channel dynamics near the stability threshold than either traditional hydrodynamic or system identification methods used alone. The specific objectives of the present investigation are:

(1) The detection and analysis of the hydrodynamic behaviour (frequency response) of a boiling channel from its naturally occurring fluctuations (inherent noise) using multivariate spectral analysis methods.

(2) The utilisation of steady state test data and spectral estimates to optimise the two-phase correlation coefficients of the linearised frequency domain hydrodynamics model developed in this investigation, and to improve its design capabilities.

(3) The determination of the dominant hydrodynamic interactions, and explanation of the mechanisms which cause the incipience of flow oscillations.

These objectives have general application to any commercial system which has sufficient high resolution instrumentation and data acquisition equipment to monitor and record the desired information. For a more detailed discussion on the spectral and hydrodynamic modelling methods presented in the following sections, interested readers are referred to the thesis by Romberg (1978a).

2. MULTIVARIATE HYDRODYNAMIC MODELS

2.1 *General hydrodynamic models*

The hydrodynamic behaviour of a typical boiling channel may be identified from the general multiple input multiple output (MIMO) model shown in figure 1, which relates the channel inlet flow, temperature and average power variations with the variations in the overall pressure drop and exit void fraction. Other model formulations are possible if alternative fundamental variables are chosen, but the present model has the advantage of characterising the essential mass, energy and momentum interactions between channel input and output by directly measurable variables. In general, MIMO system models are difficult to identify in the minimum least squares sense unless the equations describing the system are normal (Romberg 1978c), in which case the MIMO system model in figure 1(a) reduces to the two independent multiple input single output (MISO) sub-models shown in figure 1(b). These MISO sub-models assume that the outputs (exit void fraction and pressure drop) are independently related to the inputs, and are consistent with the assumption of decoupled energy and momentum conservation equations invoked in the theoretical model formulation.

The frequency response of the channel is defined by MISO spectral models, which are obtained by multivariate spectral analysis of the hydrodynamic measurements. A distributed linearised model is developed to relate the same input–output variables, and to simulate mathematically the frequency dependent hydrodynamic infrastructure of the channel. The derivation of these models, denoted spectral and mathematical models respectively, are outlined in the following sections. The procedures for interactively optimising these models to identify the mechanisms causing the flow oscillations, are discussed in section 2.4.

2.2 *Spectral models*

It is not possible within the scope of this paper to give a detailed presentation of spectral analysis theory, and therefore only the equations relevant to the computation of the spectral

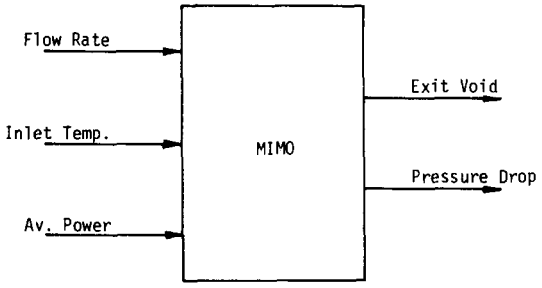

a) MIMO Model of Boiling Channel

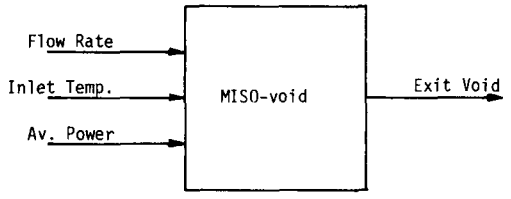

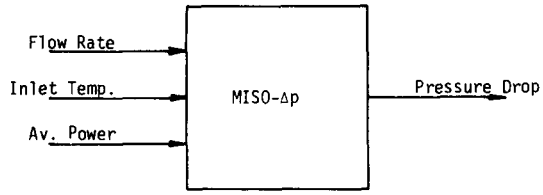

b) Equivalent MISO Sub-system Models

Figure 1. Multivariate models of a boiling channel.

estimates from their associated correlation functions are presented. Interested readers are referred to standard texts such as Jenkins & Watts (1968) and Bendat & Piersol (1971) for further details.

The cross-correlation function for an arbitrary bivariate stationary system is defined in terms of the random input variable $x_1(t)$ and output variable $x_2(t)$ as

$$R_{12}(\tau) = \lim_{T\to\infty} \frac{1}{T-|\tau|} \int_0^{T-\tau} x_1(t)x_2(t+\tau)\,\mathrm{d}t, \qquad [1]$$

where τ is the time lag between the input and output signals, and T is the total sampling time. The input autocorrelation function, $R_{11}(\tau)$, can be obtained from [1] by replacing $x_2(t+\tau)$ by $x_1(t+\tau)$, and similarly the output autocorrelation function, $R_{22}(\tau)$, can be obtained by replacing $x_1(t)$ by $x_2(t)$. The ordinary cross-spectral density estimate is given by Fourier transformation of [1]:

$$\begin{aligned}\hat{S}_{12}(f) &= \int_{-\infty}^{\infty} R_{12}(\tau)w(\tau)\,\mathrm{e}^{-j2\pi f\tau}\,\mathrm{d}\tau \\ &= \int_{-\infty}^{\infty} R_{12}(\tau)w(\tau)\cos(2\pi f\tau)\,\mathrm{d}\tau - j\int_{-\infty}^{\infty} R_{12}(\tau)w(\tau)\sin(2\pi f\tau)\,\mathrm{d}\tau \qquad [2] \\ &= \hat{C}_{12}(f) - j\hat{Q}_{12}(f),\end{aligned}$$

where $\hat{C}_{12}(f)$ and $\hat{Q}_{12}(f)$ are the co-spectral and quad-spectral density estimates respectively, and $w(\tau)$ is the lag window. The input and output power spectral density estimates ($\hat{S}_{11}(f)$ and $\hat{S}_{22}(f)$) are obtained from [2] by replacing $R_{12}(\tau)$ by $R_{11}(\tau)$ and $R_{22}(\tau)$ respectively. The cross-spectral and input power-spectral density estimates are related by the system transfer function according to the equation:

$$\hat{S}_{12}(f) = \hat{S}_{11}(f)\hat{H}_{12}(f),$$

with phase angle,

$$\hat{\psi}_{12}(f) = \arctan\left(-\hat{Q}_{12}(f)/\hat{C}_{12}(f)\right) \qquad [3]$$

In practice the cross-spectral density estimates (hence transfer function estimates) are contaminated by "extraneous" noise sources, and a measure of the coherent information transferred between the input and output signals is given by the ordinary coherence function, which is given by:

$$\hat{\gamma}^2_{12}(f) = \frac{|\hat{S}_{12}(f)|^2}{\hat{S}_{11}(f)\hat{S}_{22}(f)}. \qquad [4]$$

The coherence estimates should be close to unity for reliable cross-spectral density estimates, and in order to achieve this the following important considerations should be noted (Jenkins & Watts 1968, Romberg 1978a):

(1) The pairs of signals are bandpass filtered to remove the d.c. level and frequencies above the sampling (Nyquist) frequency. This avoids errors due to "aliasing". The filters should be identical to minimise phase distortion in the frequency bandwidth of interest.

(2) The correlation functions are weighted by a suitable lag window to minimise the "leakage" of spectral information caused by discontinuities associated with the truncation of the correlation functions. The ability of a lag window to resolve the component frequencies is determined by its resolution bandwidth, and a "window closing" technique is used to obtain the optimum bandwidth (Jenkins & Watts 1968).

(3) The cross-correlation functions are aligned to minimise the bias in the cross-spectral density estimates caused by transport delays inherent in the system. This alignment involves shifting the $\tau = 0$ axis to the maximum (or minimum) in the cross-correlation function. Bias errors in the computation of the ordinary cross-spectral density estimates result in misalignment of the partial cross-spectral density vectors in the MISO sub-models.

For the MISO systems, [1] is replaced by the matrix equation:

$$S_M(f) = S_{MM}(f)H_M(f), \qquad [5]$$

in which the transfer function relating the jth input and the output (N, $N = M + 1$, M inputs) is computed from its respective partial spectral density estimates:

$$\hat{P}_{jN:M-1}(f) = \hat{P}_{ij:M-1}(f)\hat{H}_{jN}(f). \qquad [6]$$

The partial spectral density estimates are computed from the ($N \times N$) augmented matrix of the input–input and input–output ordinary spectral density estimates using an algorithm which was developed as part of this investigation (Romberg 1978a, 1978b), and which obviates the need to invert complex matrices as in traditional multivariate spectral analysis methods. The partial

coherence estimates are calculated from their respective partial spectral density estimates by the equation:

$$\hat{\gamma}^2_{jN:M-1}(f) = \frac{|\hat{P}_{jN:M-1}(f)|^2}{\hat{P}_{jj:M-1}(f)\hat{P}_{NN:M-1}(f)}, \quad [7]$$

and the multiple coherence estimates by:

$$\hat{\gamma}_2(f) = 1 - \hat{P}_{NN:M}(f)/\hat{S}_{NN}(f). \quad [8]$$

It should be noted that the direct application of spectral analysis methods is not valid if there is feedback between the output and the input, and the inputs are measured inside the feedback loop (Priestley 1969). The feedback problem arises in the present context if the bypass in parallel with the boiling channel has a small bypass/channel flow ratio. The test channel used in this investigation had a bypass ratio of about 50:1, which ensured that it was operating in a parallel channel mode (Carver 1969), and enabled feedback effects on the spectral results to be neglected.

It should also be noted that the lag (or spectral) window smooths the spectral model transfer function estimates (e.g. Romberg & Rees 1975), and thus the input–output cross-spectral density functions are used in the spectral/mathematical model comparisons to partially compensate for this problem.

2.3 *Mathematical model*

Numerous time and frequency domain models have been developed to investigate incipient flow instabilities in boiling channels (see reviews by Neal & Zivi 1965, Grumbach 1969). A detailed mathematical model of the two-phase flow structure requires six conservation equations (three for each phase), plus constitutive equations to define the fluid properties of the system, and mass, energy and momentum transfer relationships at the vapour/liquid boundaries (Boure *et al.* 1973, Boure 1975). However, since detailed transfer relationships (laws) are still not available, the current use of six conservation equation models is not yet possible, and they are only useful in clarifying the assumptions of existing simplified models, which usually assume one-dimensional turbulent flow.

A general mathematical model aims to simulate the flow structure in five interconnected hydrodynamic regions: a single phase subcooled liquid region, a wall void region, a subcooled boiling region, a saturated boiling region, and a superheated vapour region. The model developed in the present investigation is only concerned with the hydrodynamics of the single phase subcooled liquid, subcooled boiling and saturated boiling regions. It is based on a linearised solution of the cross-section averaged equations for the conservation of mass, energy and momentum of the two-phase (vapour/liquid) mixture. A computer program (LOCO—a linearised model for analysing the onset of coolant oscillations in boiling channels) has been developed to perform the numerical calculations. The program calculates the frequency response relationships between perturbations in channel inlet flow rate, temperature, pressure, average power (inputs) and the overall pressure drop, exit void fraction (outputs). The inputs may be frequency independent ("white noise") for transfer function and stability calculations, or frequency dependent real or complex experimental data for frequency response calculations.

2.3.1 *Conservation equations.* The one-dimensional equations for the conservation of mass, energy and momentum may be written as:

Mass:
$$\frac{\partial}{\partial z}\{G\} + \frac{\partial}{\partial t}\{\rho_l(1-\alpha) + \rho_g\alpha\} = 0; \quad [9a]$$

Energy:
$$\frac{\partial}{\partial z}\{G_l h_l + G_g h_g\} + \frac{\partial}{\partial t}\{\rho_l(1-\alpha)h_l + \rho_g\alpha h_g - p\} = Q; \quad [9b]$$

Momentum:

$$\frac{\partial}{\partial z}\{G_l U_l + G_g U_g\} + \frac{\partial}{\partial t}\{G\} + \frac{K_f}{2}\frac{G^2\phi^2}{\rho_l} + \{\rho_l(1-\alpha) + \rho_g\alpha\}\, g\cos\theta = -\frac{\partial p}{\partial z}, \qquad [9c]$$

where the symbols (see Nomenclature) denote cross-section averaged variables, and the kinetic and potential energy terms in the energy equation are neglected. Equations [9] are solved as follows:

(1) The channel variables (pressures, mass fluxes, void fraction, etc.) are perturbed with respect to time, and the product terms linearised (terms higher than the first order are neglected).

(2) The perturbed variables are transformed into the frequency domain by Laplace transformation,

$$F(z, s) = \tilde{F}(z) = \int_0^\infty F^*(z, t)\, e^{-st}\, dt, \qquad [10]$$

where $F(z, t) = F^0(z) + F^*(z, t)$, $s(= \sigma + j\omega)$ is the complex Laplace operator, and zero initial conditions are assumed;

(3) The first order differential equations are integrated spatially over a small space node (axial length $\Delta z \times$ channel cross-sectional area) using the forward difference equation

$$\int_0^{\Delta z} \frac{\partial \tilde{F}(z)}{\partial z}\, dz = \tilde{F}_{i+1} - \tilde{F}_i \qquad [11]$$

and the trapezoidal rule,

$$\int_0^{\Delta z} \tilde{F}(z)\, dz = \frac{\Delta z}{2}(\tilde{F}_{i+1} + \tilde{F}_i).$$

(4) The fluid properties and heat flux at the wall/coolant interface are assumed spatially invariant within the space node, and all fluid properties except the vapour density (ρ_g) are assumed to be time invariant.

Finite difference equations are derived for the steady state and dynamic analysis of the thermal non-equilibrium two-phase flow through the subcooled boiling region of the channel. Specification of certain parameters and variables reduces these equations to simpler forms for analysis of the single phase liquid and saturated boiling regions.

2.3.2 *Empirical correlations.* In addition to the above conservation equations, the following empirical correlations are used to predict the onset of subcooled boiling, and model the flow characteristics in the two-phase region of the channel:

(1) Subcooled boiling boundary correlation (Saha & Zuber 1974)

$$\mathrm{Nu} = \frac{h_{lo} D_e}{k_l} = 455, \qquad \mathrm{Pe} < 70{,}000$$

$$\mathrm{St} = \frac{h_{lo}}{GC_{pl}} = 0.0065, \qquad \mathrm{Pe} > 70{,}000. \qquad [12]$$

The local liquid enthalpy for the onset of subcooled boiling is given by

$$h_o = h_f - \frac{C_{pl} q_{wo}}{h_{lo}},$$

and the subcooled boiling boundary occurs when

$$h_l^o(z_o) = h_o. \tag{13}$$

Note that Nu = Pe × St, and hence 455 = 70,000 × 0.0065.

(2) Subcooled boiling region liquid enthalpy profile (Kroeger & Zuber 1968).

Exponential correlation—

$$h_l^+ = (h_l - h_o)/(h_f - h_o) = 1 - \exp(-h^+). \tag{14}$$

Hyperbolic tangent correlation—

$$h_l^+ = \tanh(h^+), \tag{15}$$

where $h^+ = (h - h_o)/(h_f - h_o)$.

(3) Slip correlation (Zuber & Findlay 1965)

$$S = \frac{\langle 1 - \alpha \rangle}{K_o - \langle \alpha \rangle}, \tag{16}$$

where

$$K_o = \text{Bankoff factor} = \frac{\langle \alpha \rangle \langle J \rangle}{\langle \alpha U_g \rangle} = \frac{1}{C_o + \dfrac{V}{\langle J \rangle}},$$

$$V = \text{weighted mean vapour drift velocity} = \frac{\langle \alpha \Delta U_g \rangle}{\langle \alpha \rangle}, \text{ and} \tag{17}$$

$$C_0 = \text{distribution parameter} = \frac{\langle \alpha J \rangle}{\langle \alpha \rangle \langle J \rangle}.$$

(4) Two-phase friction multiplier (Beattie 1971)

$$\phi^2 = 1 + a[(\rho_l/\rho_g - 1)x]^b G^c. \tag{18}$$

(5) Heater/coolant dynamics. The fundamental mode heater/coolant dynamics are governed by the overall time constant τ_H, which is given by (Romberg 1978a)

$$\tau_H = f_{ht}\theta_T/h_t, \tag{19}$$

where f_{ht} is a heat transfer factor, θ_T is the heater thermal capacitance per unit surface area, and h_t is the heat transfer coefficient. The liquid phase heat transfer coefficient is given by the Dittus–Boelter correlation. The two-phase heat transfer coefficient is given by the sum of the liquid and vapour phase heat transfer coefficients, the latter having the form proposed by Davis & David (1964).

2.3.3 *Numerical integration.* The channel is divided into a number of volume elements, and the continuity in flow conditions between successive elements is provided by coupling equations at the boundary (or interface). In a similar manner, the flow conditions between the single phase and two-phase regions are coupled by mass, energy and momentum conservation equations at the boiling boundary. The steady state and dynamic relationships between

variables at the channel inlet and exit are calculated by piecewise integration along the channel. The relevant finite difference equations are given in Romberg (1978a).

A schematic diagram of the computational procedure used in the boiling channel model is given in figure 2. The top blocks represent the nodal mass and energy conservation equations, and the lower blocks represent the nodal momentum conservation equations. The program subdivides each volume element into smaller nodes and subnodes, particularly near the boiling boundary, where small spatial steps are required to ensure numerical stability of the steady state and dynamic calculations in the two-phase region of the channel.

The steady state calculations are performed first to evaluate the coefficients in the dynamic equations, and to obtain the overall pressure drop, which is a function of the single phase and two-phase momentum, friction and gravitational pressure drops, as well as local restriction pressure drops due to expansions, contractions, orifices, etc. at the section boundaries.

In the dynamic analysis, the piecewise calculation of the local perturbed variables is performed for specified values of the complex Laplace operator. The perturbations at the channel inlet travel through the single phase region to the boiling boundary, where the perturbations are transmitted to the vapour and liquid phases and travel to the channel exit. The overall perturbed pressure drop is a vector summation of the single phase and two-phase region pressure drops, which in turn are vector sums of their respective momentum, friction, gravitation and restriction components. It can be seen from figure 2 that the overall perturbed pressure drop is linearly related to the inlet mass flux, pressure, enthalpy, and average power density perturbations by the equation

$$\Delta\tilde{p} = \tilde{H}(\Delta p, G_1)\tilde{G}_1 + \tilde{H}(\Delta p, p_1)\tilde{p}_1 + \tilde{H}(\Delta p, h_1)\tilde{h}_1 + \tilde{H}(\Delta p, \langle Q_s\rangle)\langle\hat{Q}_s\rangle, \qquad [20]$$

where $\tilde{H}(y, x)$ represents the spatially integrated frequency dependent transfer function between an arbitrary input variable (x) and output variable (y). The first term $\tilde{H}(\Delta p, G_1)$ in [20] is the channel "hydraulic impedance" (Anderson 1970), and is the dominant term in the frequency range of interest (0.1–2 Hz). The remaining three terms are respectively, the compressibility, liquid enthalpy (or temperature) and heat source/coolant contributions, and usually have only a marginal effect on the overall pressure drop perturbation in most heat transfer systems.

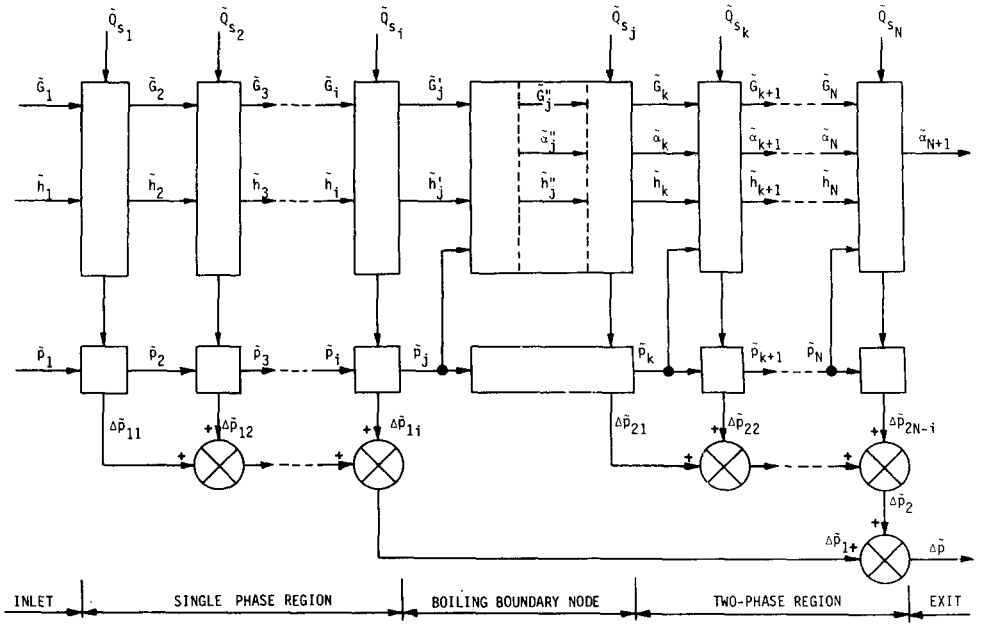

Figure 2. Schematic diagram of boiling channel model.

However, they are included in the present model for the more general system analysis discussed in section 2.1 and figure 1.

2.3.4 *Parallel channel stability criterion.* A channel will exhibit self-sustained flow oscillations with fundamental frequency f_o when

$$\Delta p(f_o) = \Delta p_1(f_o) + \Delta p_2(f_o) = 0, \qquad [21]$$

that is, it satisfies the linear "instability threshold" condition of constant pressure differential across all the channels in parallel. The boundary condition [21] is satisfied when the perturbed single phase and two-phase pressure drops ($\Delta p_1(f_0)$ and $\Delta p_2(f_0)$ respectively) are 180° out of phase. This implies that, as assumed by most hydrodynamic models (e.g. Jones 1961, Davies & Potter 1967, Takahashi & Shindo 1971, Spinks 1971, Yadigaroglu & Bergles 1972), the locus of the hydraulic impedance function $\tilde{H}(\Delta p, G_1)$, [20], passes through the origin of its Argand diagram at frequency f_o, i.e.

$$H(\Delta p, G_1, f_o) = H_o(\Delta p, G_1) = 0. \qquad [22]$$

It should be noted that a major advantage of assessing system stability by the hydraulic impedance function $H(\Delta p, G_1)$ is that it is defined in terms of measurable variables (inlet mass flux, overall pressure drop), whereas the open loop stability criteria of feedback models are not directly measurable, since they are based on perturbed variables which are functions of an experimentally indeterminate boiling boundary position.

2.4 *Modelling procedures*

It is generally recognised that although theoretical models are able to give relatively detailed information on the mechanisms underlying the hydrodynamic behaviour of a channel, the results are sensitively dependent on the validity of the empirical correlations (Bjorlo *et al.* 1967). By contrast, the spectral models derived from inherent noise measurements, whilst being powerful methods for channel hydrodynamic analysis, do not contain structural information about the mechanisms underlying the response. In this investigation, the complementary advantages of both models are used by coupling them interactively as in system identification studies (Eykhoff 1974, Seinfeld & Lapidus 1974). However, in contrast with the empirical parameter estimates of "black box" models or the lumped parameters of macroscopic physical models used in system control studies, the parameters (coefficients) of the two-phase correlations, [12]–[19], are only varied within the ranges suggested by the heat transfer literature, so that their "physical" significance is retained.

The basic identification procedure is depicted in figure 3, and the steps are summarised as follows:

(1) The mathematical model calculations are performed at the same steady state conditions (inlet flow, temperature, pressure, average power) as monitored experimentally. A parametric survey is made to assess the effects of the subcooled boiling, two-phase slip and friction multiplier coefficients on the agreement between the predicted and measured steady state exit void fraction and pressure drops over the range of channel power levels.

(2) The two-phase slip and friction correlation coefficients are optimised by minimising the errors between the measured and calculated exit void fraction and channel pressure drop at a power level near the instability threshold. The functional dependence of these coefficients on the subcooled boiling boundary position, that is, the subcooled boiling boundary Nusselt/Stanton numbers in [12], is obtained by performing the optimisation over a range of Nusselt numbers.

(3) The subcooled boiling Nusselt number is optimised by minimising the mean square errors between the flow-pressure drop cross-spectral density (CSD) modulus estimates of the

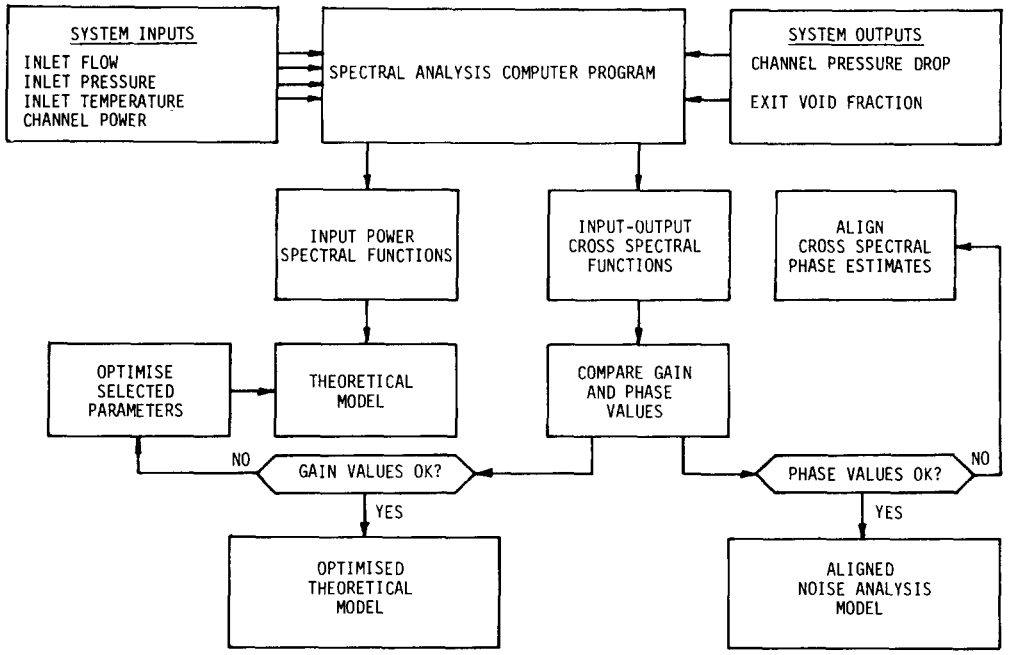

Figure 3. System identification procedure.

noise model and the mathematical model, where the latter estimates are obtained by perturbing the mathematical model with the flow noise power spectral density estimates, as shown in figure 3. These calculations were performed for both the exponential and hyperbolic tangent subcooled boiling liquid enthalpy correlations, [14] and [15].

(4) The influence of the heater/coolant dynamics, [19], is assessed by varying the factor (f_{ht}) over a range of values, and noting the improvement in the mean square errors of the flow-pressure drop and flow-exit void CSD modulus estimates.

(5) The optimised mathematical model phase angles become the reference for aligning the phase estimates of the spectral model, and are used to assess the flow stability of the channel, as well as the mechanisms (pressure drop components) which tend to drive the channel unstable.

These procedures are discussed in more detail in section 5, where the model results are presented.

3. TEST FACILITY AND PROCEDURES

3.1 *General description*

A centrifugal pump circulated Freon 113 coolant around the primary circuit of a rig, which consisted of five test channels and a large bypass connected in parallel between headers at the inlet and outlet. The pump discharge was connected to the inlet header, and the outlet header was connected to a vapour condenser and a subcooler, which condensed and subcooled the Freon 113 before its return to the pump inlet.

The series of experiments described in the following section were performed on only one of the five test channels. The other four channels were used to provide additional bypass flow for controlling the pressure drop across the test channel. A more detailed description of the test facility and procedures is given in Romberg (1978a).

3.2 *Test channel and instrumentation*

A schematic diagram of the test channel and its associated instrumentation is shown in figure 4. The test channel consisted of an inlet pipe with a venturi flowmeter, a heated section

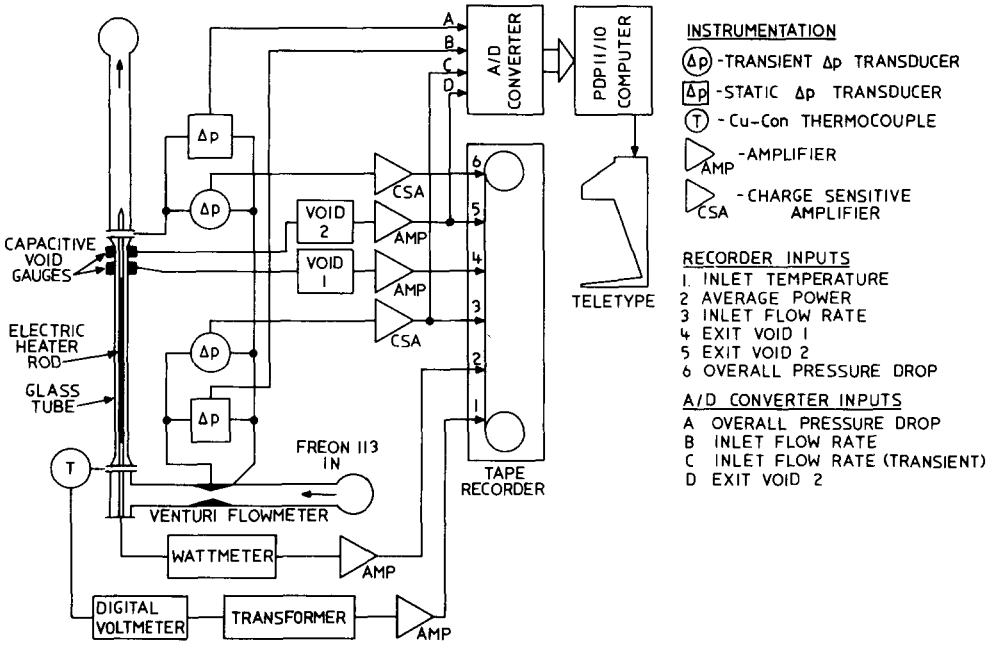

Figure 4. Schematic diagram of test channel and instrumentation.

made of Pyrex glass tube with a concentric electric heater rod, and a glass riser section. The principal dimensions of the test channel are given in Appendix 1.

The measurements made on the test channel included the inlet flow rate, temperature, pressure, power input, channel pressure drop and exit void fraction (figure 4). Capacitive and piezoelectric transducers were used to measure respectively the static and dynamic differential pressures. The inlet temperature was measured with copper–constantan thermocouples and the power input with a Hall effect wattmeter. Two capacitive void gauges were installed near the channel exit to measure the void fraction and vapour transit times. The gauges work on the principle that the different dielectric constants of the flowing vapour and liquid phases induce capacitive changes between the plates of the cylindrical capacitor, and these changes are converted to voltage changes by an electronic circuit. Air–Freon and boiling Freon tests on a calibration rig showed that the voltage outputs of the gauges were linear functions of the void fraction over the entire range from zero to unity.

3.3 *Test procedure and data acquisition*

After a warm-up period of 1 h, in which entrained air was removed from the Freon, the rig conditions were set for the first experiment. Data logging was commenced by initiating the control program in the PDP11/10 minicomputer and starting the magnetic tape recorder (figure 4). The minicomputer also controlled a Hewlett Packard on-line correlator, which calculated the variance of the venturi flowmeter noise. The variance was averaged over 1 min, and twenty data samples were logged during each experiment (about 22 min total). At the end of each recording sequence, the power was incremented and the procedure repeated until flow oscillations were observed. The inverse variance of the flowmeter noise was plotted as a function of the power input for each experiment, and gave a sensitive indication of the change in rig conditions with power. This plot proved an effective aid for manual control of the rig by giving an on-line prediction of the instability threshold power for the onset of flow oscillations.

4. TEST RESULTS

4.1 *Steady state*

The change in steady state mass flow, inlet temperature, exit void fraction and pressure drop with increments in heater power input is tabulated in Appendix 2, and plotted in figure 5. The

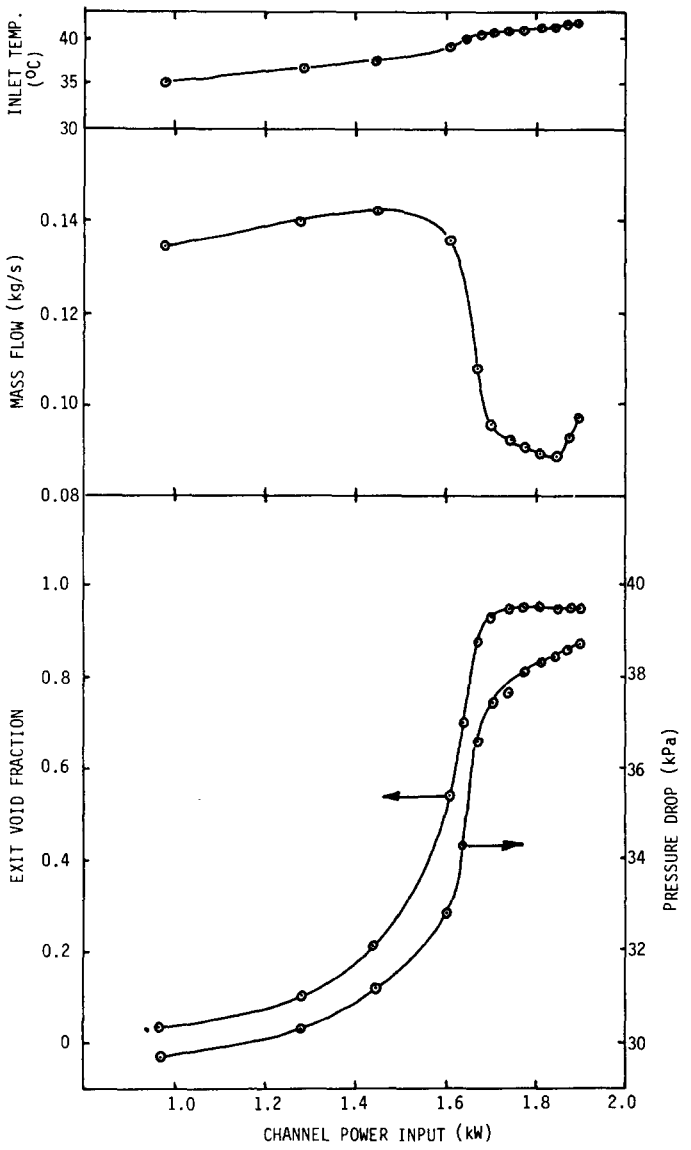

Figure 5. Experimental steady state results.

inlet temperature had an upward drift of about 6°C/kW for the 8-h duration of the experiments, and this was possibly caused by the changes in both the operating and ambient conditions. There was a characteristic reduction in mass flow to satisfy the boundary condition of almost constant header-to-header pressure drop, and this resulted in a correspondingly rapid rise in the void fraction at the channel exit. The asymptotic limit of 95 per cent void fraction at the higher power levels suggested little or no slip between the vapour and liquid phases.

4.2 *Inverse variance-power map*

The inverse variance-power maps obtained from on-line computations and reanalysis of the flow noise recorded on magnetic tape are given in figure 6(a) and 6(b) respectively. The essential difference between the two results is the bandpass filter settings. The on-line computations were bandpass filtered in the range 0.1–2.0 and gave an instability threshold power (ITP) of 1.92 kW, whereas the off-line tape analysis had bandpass filter settings of 0.125–1.125 Hz, and gave an ITP of 1.88 kW. This difference in ITP is primarily due to the contribution of broadband turbulent noise in the frequency range of interest.

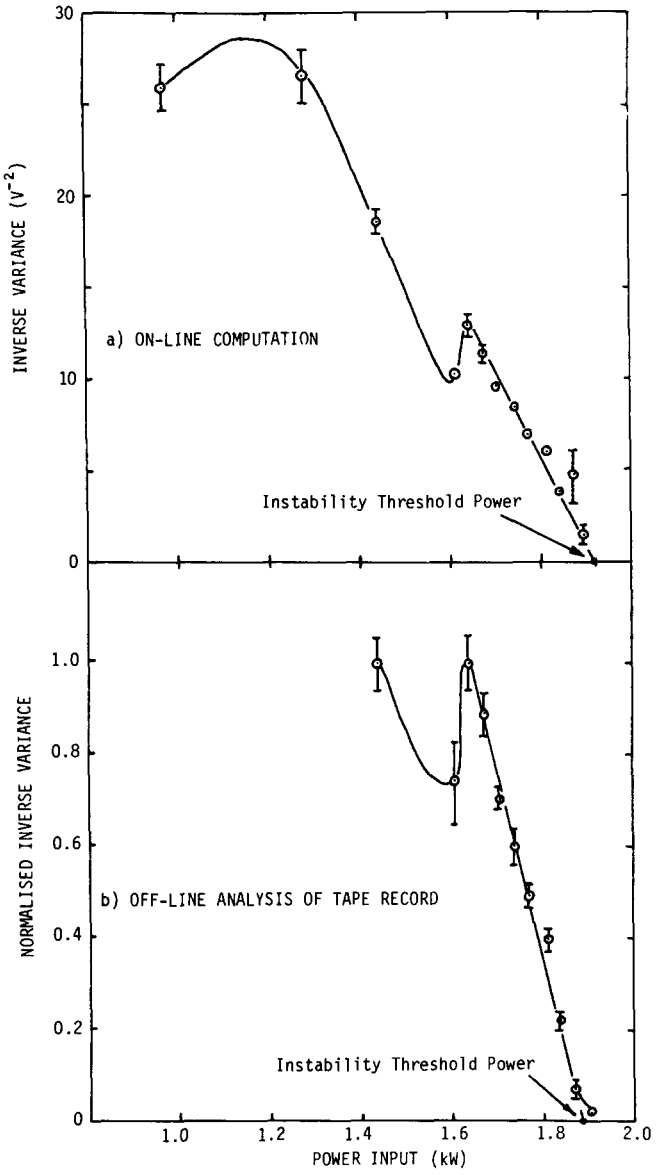

Figure 6. Inverse variance-power map of flowmeter noise.

There has been some speculation regarding the use and validity of inverse variance as a means of predicting the ITP. Bjorlo *et al.* (1967) suggests that inverse variance weighted by the square of the mean flow gives more accurate predictions of the ITP, and this method is generally adopted in practice (e.g. Gall 1973). Brimley *et al.* (1976) used the inverse standard deviation weighted by the mean flow, and questioned its usefulness as a method for predicting the ITP. In this context, the authors' experience and conclusions regarding prediction of the ITP by the inverse variance method in the present tests are pertinent, and may be summarised as follows:

(1) The inverse variance was a linear function of the power level prior to the onset of flow oscillations (figure 6), and gave satisfactory predictions of the ITP.

(2) The mean flow was not a linear function of power (as in most constant pressure drop systems), and thus the inverse variance weighted by the square of the mean flow results in a non-linear function of power, which may not give accurate predictions of the ITP by extrapolation to zero weighted inverse variance.

(3) Care should be taken to minimise the effects of broadband turbulent noise both at the transducer and signal processing stages.

(4) Ensemble averaging of the variance estimates is important for the minimisation of statistical errors.

The last point is related to the fact that the variance is equivalent to the summation of its associated power spectral density estimates, and the variance of these estimates is related to the resolution bandwidth by (Jenkins & Watts 1968)

$$\text{variance} \times \text{bandwidth} = \text{constant}. \qquad [23]$$

Thus, subdividing the total record into a number of disjoint records has the effect of increasing the bandwidth and reducing the variance of the spectral (hence variance) estimates.

4.3 *Evolutionary amplitude spectra*

The development of unstable flow conditions in the test channel is graphically illustrated by the isometric plot of the flow noise amplitude spectra shown in figure 7, which indicates that unstable conditions occur between 1.84 and 1.87 kW (slightly lower than the predicted value of 1.88 kW by the inverse variance method). The channel has a resonant frequency of 0.56 Hz at 1.87 kW, which agrees with the oscillation period of 1.82 sec (0.55 Hz) measured with a stopwatch from visual observations. The fundamental and higher mode limit cycle oscillations are more evident in the amplitude spectra at the higher power levels (1.87 and 1.90 kW). The non-linear limit cycle conditions at these power levels cannot, of course, be analysed by linearised modelling techniques. The spectra of the other variables showed similar trends (Romberg 1978a).

4.4 *Cross-spectral density estimates (CSDE)*

The amplitude spectrum at 1.84 kW indicates a damped harmonic system, and the channel behaviour at this power level was studied in greater detail with the multivariate spectral analysis methods outlined in section 2.2. The signals were analysed in pairs at a recorder replay speed sixteen times the original recording speed, and were bandpass filtered in the frequency range 1–18 Hz (0.125–1.125 Hz real time). The Hewlett-Packard correlator settings were 32 × 1024 ensembles and 10 ms lag interval. A Parzen lag window was used to smooth the spectral density estimates, and the window closing technique gave an "optimum" resolution bandwidth

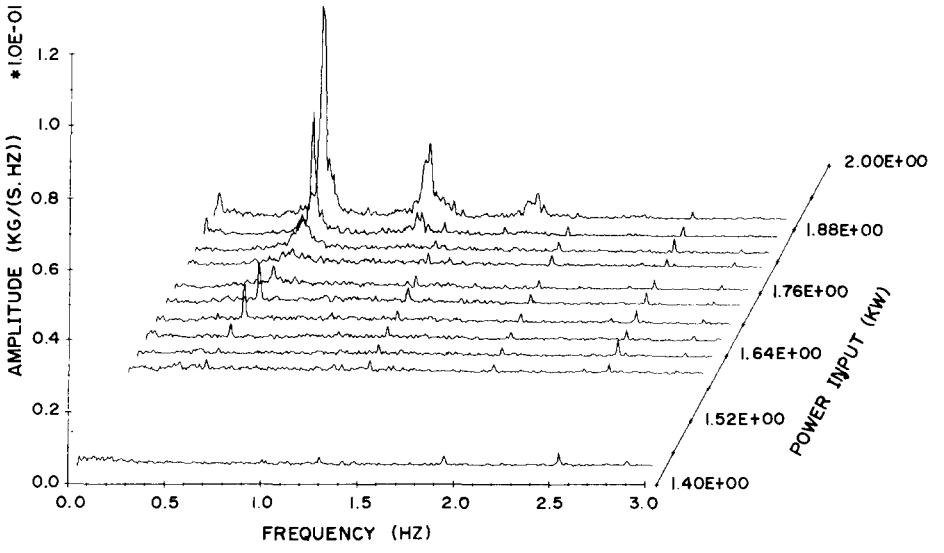

Figure 7. Evolutionary amplitude spectra of flowmeter noise.

of 0.204 Hz, equivalent to 57 lags or 5 periods. This window was selected for its minimum leakage characteristics (Jenkins & Watts 1968).

The ordinary and partial CSDE (modulus and phase) and the ordinary, partial and multiple coherence estimates for the MISO-void and MISO-Δp sub-models (figure 1) were computed as discussed in section 2.2, and the results are presented in figures 8 and 9 respectively. The essential points that could be noted from these results are summarised as follows:

(1) All the moduli of the ordinary CSDE have maxima between 0.54 and 0.56 Hz, which are consistent with the observed resonant frequency of the channel.

(2) The *ordinary* coherence estimates suggest that the inlet flow and temperature have significant influence on the outputs (exit void, pressure drop) at the resonant frequency, whereas the channel power has only a marginal influence.

(3) However, the *partial* coherence estimates show that only the inlet flow has a significant effect on the outputs, and thus the MISO sub-models (figure 16) may be further reduced, in this case at least, to flow-exit void and flow-pressure drop SISO sub-models.

The high ordinary and low partial coherence estimates between the inlet temperature and the outputs indicates that it is related dynamically to the inlet flow. It can be shown (Romberg 1978a) that the fundamental mode dynamics of the thermocouple response is given by

$$\tilde{\theta} = \tilde{H}(\theta, T)\tilde{T} - \tilde{H}(\theta, W)\tilde{W} + \tilde{H}(\theta, Q_s)\tilde{Q}_s, \qquad [24]$$

where the first term on the r.h.s. is the contribution by the fluid temperature noise (the desired measurement), the second term is the flow rate contribution via heat transfer at the thermocouple/fluid interface, and the third term is the contribution due to self heating effects which, for this type of passive thermocouple, is usually negligible. The influence of the flow rate noise on the thermocouple noise is shown in figure 10. The high coherence (0.87) between these measurements at the resonant frequency confirms that they are not sufficiently independent for the MISO sub-models to be valid. Therefore in the present case, the inlet temperature cannot be used as an input in conjunction with the inlet flow, and is eliminated from the model. A measure of the true fluid temperature noise is given by the residual noise spectra in figure 10.

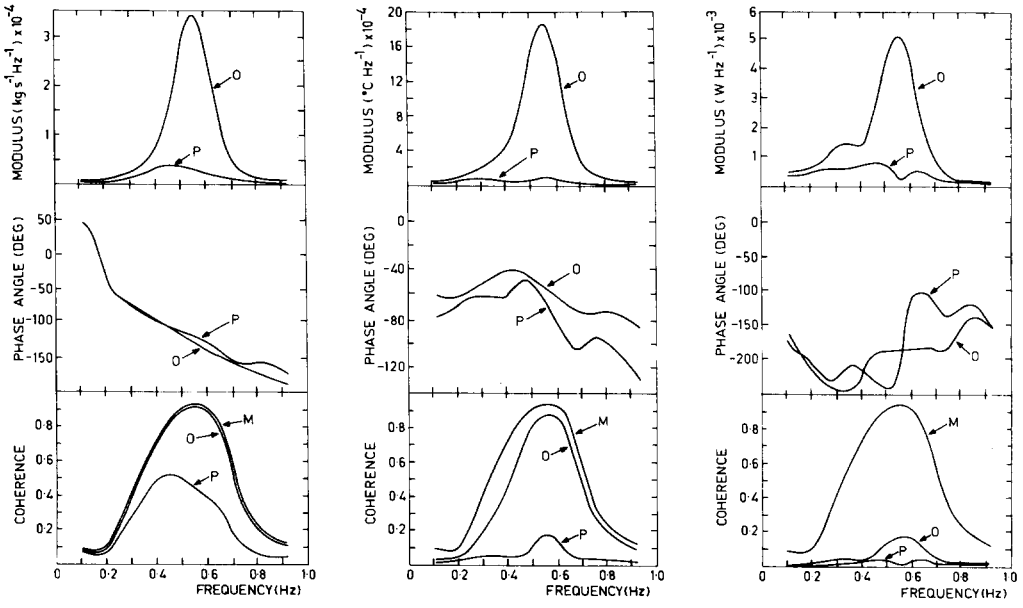

(a) Flow-exit void. (b) Inlet temp-exit void. (c) Power-exit void.

Figure 8. Cross-spectral density and coherence estimates for MISO-void model (1.84 kW) (O = ordinary: P = partial: M = multiple).

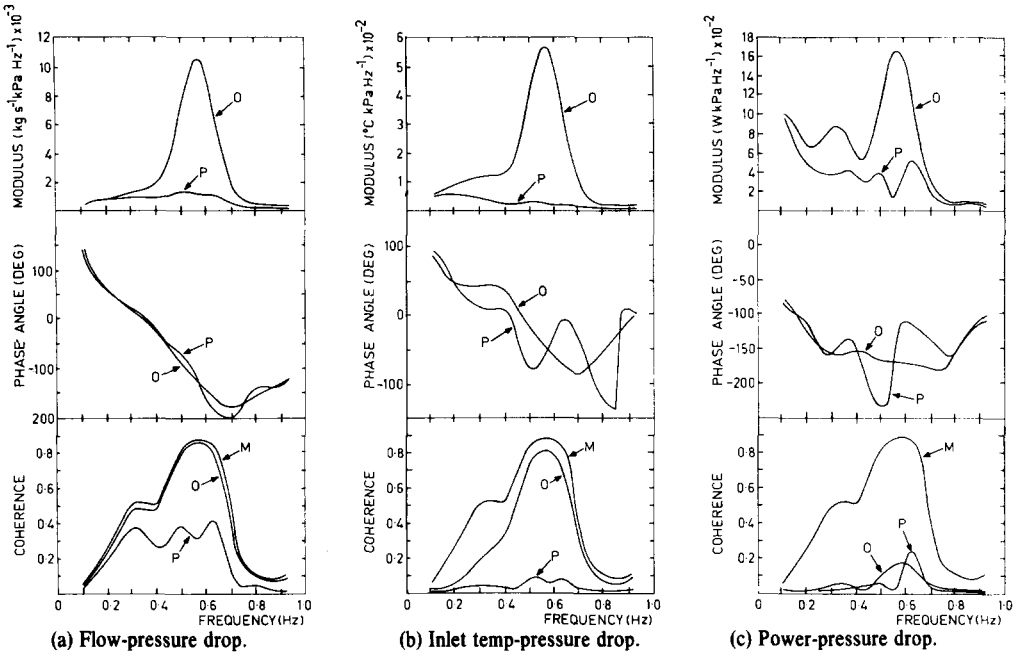

(a) Flow-pressure drop. (b) Inlet temp-pressure drop. (c) Power-pressure drop.

Figure 9. Cross-spectral density and coherence estimates for MISO-Δp model (1.84 kW) (O = ordinary: P = partial: M = multiple).

5. THEORETICAL RESULTS

5.1 *Parameter sensitivity analysis*

As outlined in section 2.4, the initial step in the mathematical simulation procedure is the prediction of the steady state exit void fraction and pressure drop, and the sensitivity of the predicted values to variations in the two-phase correlation coefficients, [12]–[19], between the limits suggested by the heat transfer literature. The limits used in this parameter sensitivity analysis are tabulated in Appendix 3, and the theoretical predictions are compared with the experimental void and pressure drop results in figure 11.

Figure 11(a) shows the theoretical results with the subcooled boiling boundary Nusselt number based on the equivalent hydraulic diameter (Nu = 455, as assumed by Saha & Zuber

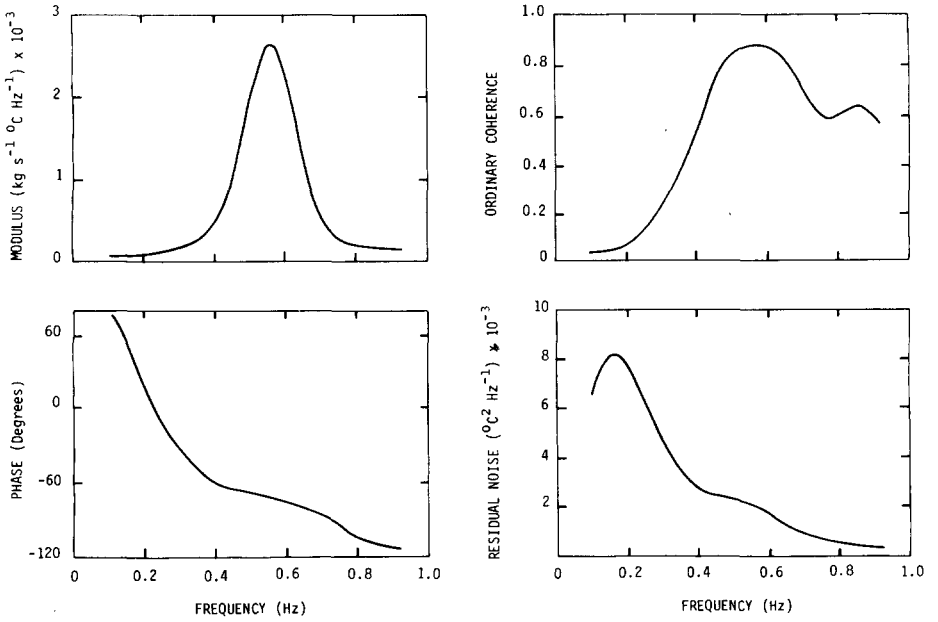

Figure 10. Influence of flow rate noise on thermocouple (1.84 kW).

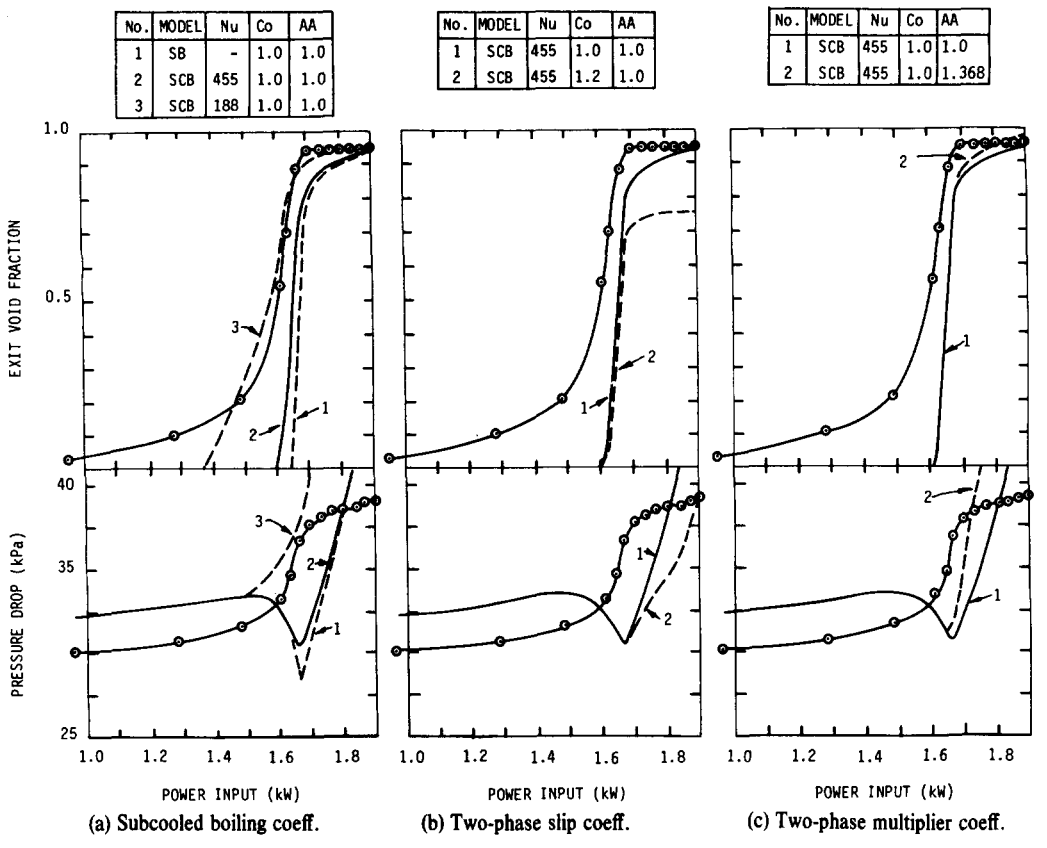

(a) Subcooled boiling coeff. (b) Two-phase slip coeff. (c) Two-phase multiplier coeff.

Figure 11. Effect of correlation coefficients on theoretical exit void and pressure drop results (—⊙—experimental: ═══theoretical: SB = saturated boiling: SCB = subcooled boiling).

1974) and the equivalent heated diameter (Nu = 188). The case with Nu = 455 yields an exit void fraction which is lower than experiment, and is only marginally better than the case which assumes saturated boiling only. The case with Nu = 188 gives much better agreement, except at the very low power levels. Visual observations noted during the experiments did not detect boiling on the heater surface at the two lowest power levels, and it is possible both the void gauges and the differential pressure transducer were measuring the presence of residual entrained air at these conditions. The mismatch between the measured and calculated exit void fraction is also reflected in the pressure drop results. The cases with Nu = 455 and saturated boiling have minima in their pressure drop loci at 1.65 kW. Inspection of the calculated steady state pressure drop components below this power level shows that the decrease in gravitational pressure drop due to boiling is greater than the increase in momentum and friction pressure drops, whereas this situation is reversed above this power level. The case with Nu = 188 has no minimum because of the predominance of the momentum and friction pressure drop components.

The inclusion of slip ($C_0 = 1.2$, figure 11b) results in a lower exit void fraction, particularly at power levels above 1.70 kW. The significance of this result is that a larger fraction of the thermal energy flux ([9b]) is dispersed in accelerating the vapour phase rather than in producing more voids.

The insertion of a non-homogeneous two-phase friction multiplier ($a = 1.368$, figure 11c) results in a higher friction pressure drop component, and an overestimation of the pressure drop at power levels above 1.70 kW. More recent research (Beattie 1977, Deev *et al.* 1978) suggests that, under certain conditions, there is a drag reduction mechanism associated with the two-phase flow through heated channels, and this may be simulated by allowing the coefficients in [18] to have values less than their homogeneous values (i.e. $a < i$ or $b < 1$ or $c < 0$).

In summary, it can be concluded from this parameter sensitivity analysis that:

(1) The incipience of subcooled boiling is more accurately predicted by correlation coefficients based on the equivalent heated diameter than the equivalent hydraulic diameter.

(2) There is little or no discernible slip between the vapour and liquid phases.

(3) The homogeneous two-phase friction multiplier overestimates the friction pressure drop, and may be affected by a possible drag reduction mechanism.

5.2 *Parameter optimisation procedure*

The parameter sensitivity analysis has highlighted the need for more accurate values of the subcooled boiling and two-phase correlation coefficients. (It may be noted that this sensitivity is a function of the low pressure operation (168 kPa) or high liquid/vapour density ratio.) Both sets of parameters are coupled via their influence on the axial void and pressure drop profiles, in both the steady and dynamic states. A number of methods could be adopted to "optimise" the estimates of these parameters (Romberg 1978a), but the most sensitive procedure was found to be one which used both models interactively as outlined in section 2.4 and figure 3.

The initial step in the optimisation procedure is the matching of the calculated exit void fraction and pressure drop with that measured at the power level of 1.84 kW, near the ITP. For a given value of the subcooled boiling boundary Nusselt number, the two-phase distribution parameter (C_o) and friction multiplier coefficient (a) are varied to match the experimental co-ordinate on an exit void-pressure drop plot (0.951 and 38.71 kPa, Appendix 2) at the same operating conditions. This match was performed for Nusselt number values Nu = 170, 250, 350 and 455 to span the range of interest (Nu = 188–455), and enabled the functional dependence of the distribution parameter and friction multiplier coefficient on the subcooled boiling Nusselt number to be derived using a power law least squares curve fit. These functional relationships were derived for both the exponential and hyperbolic tangent subcooled boiling liquid enthalpy correlations, [14] and [15].

The second step in the optimisation procedure is the determination of the subcooled boiling boundary Nusselt number most appropriate for the annular test channel. As noted in a previous paper (Romberg & Rees 1975) and section 2.4, this is obtained by minimising the mean square errors in the moduli of the flow-exit void and flow-pressure drop CSDE in the frequency range of acceptable coherence (0.40–0.80 Hz, figures 8a and 9a), i.e.

$$\bar{\epsilon}^2_{xy} = \frac{1}{N}\sum_{n=1}^{N}[\hat{S}_{xy}(f_n) - S_{xy}(f_n)]^2\,, \qquad [25]$$

where x = input (flow), y = output (exit void fraction or pressure drop) and N = number of frequencies (= 20). The results of this error minimisation for both the exponential and hyperbolic tangent correlations are shown in figure 12, where it can be seen that there are no minima in the flow-exit void CSD modulus mean square errors, and the flow-pressure drop CSD modulus mean square errors give an optimum subcooled boiling Nusselt number of 193 for the hyperbolic tangent correlation. Some improvement in the mean square errors is obtained by weighting the flow noise input by the respective input–output ordinary coherence estimates, [4], to account for extraneous noise sources on the input (Romberg 1978a). These results are significant because they (1) provide additional confirmation that the subcooled boiling boundary Nusselt number should be based on the equivalent heated diameter, and (2) indicate that the subcooled boiling region liquid enthalpy (hence void) profile is modelled best by the hyperbolic tangent correlation.

The corresponding values of the distribution parameter and friction multiplier coefficient for the optimum Nusselt number are $C_o = 0.9835$ and $a = 0.7557$. The optimum distribution parameter indicates that the voids are concentrated in a slower moving region near the heater surface, and the optimum multiplier coefficient tends to confirm the presence of a drag reduction mechanism.

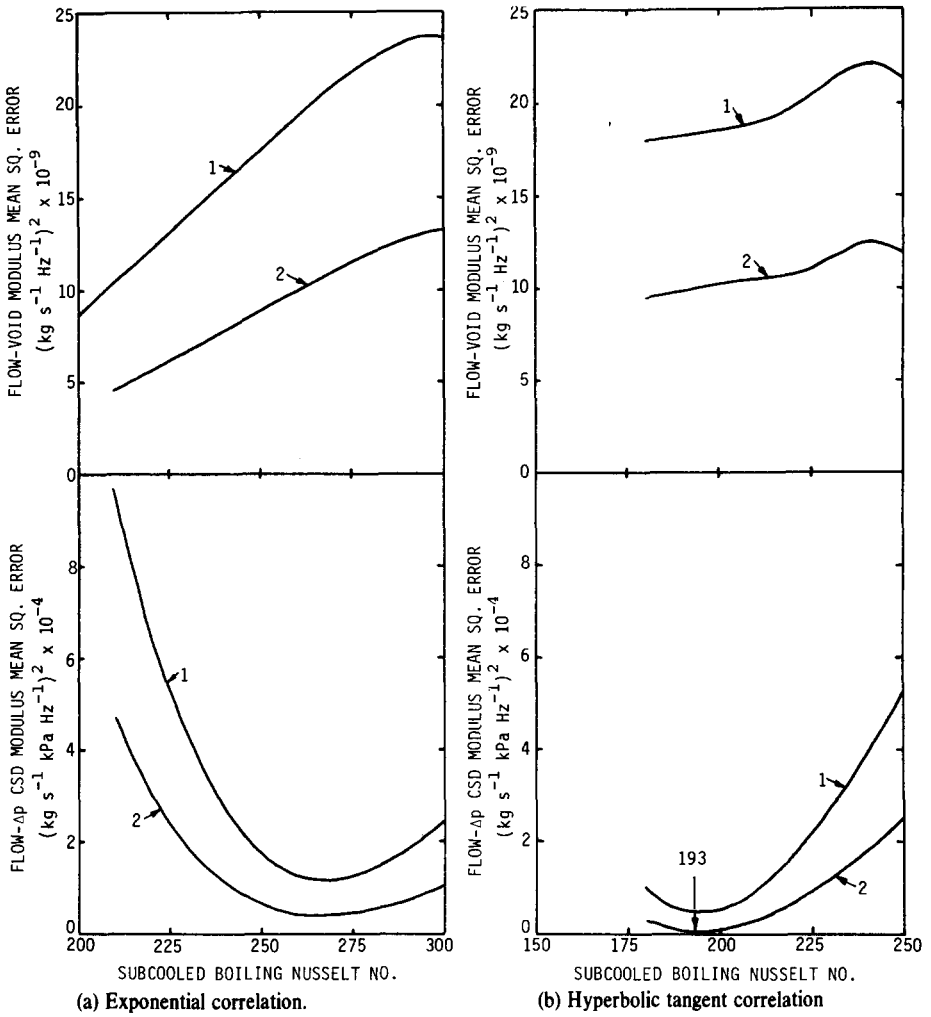

(a) Exponential correlation. (b) Hyperbolic tangent correlation

Figure 12. Optimisation of the subcooled boiling correlation Nusselt number (1.84 kW) (flow noise spectral density input: without (1) and with (2) coherence weighting).

The final step in the optimisation procedure is the assessment of the heater/coolant dynamics on the flow-exit void and flow-pressure drop CSD modulus mean square errors. This assessment is made by varying the heat transfer factor f_{ht}, [19], through a range of values with

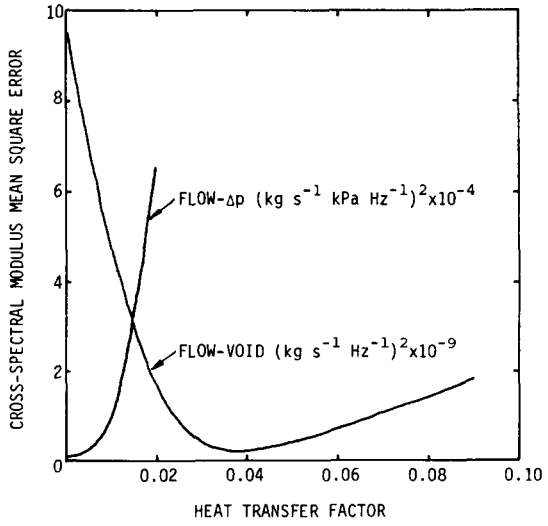

Figure 13. Optimisation of the heat transfer factor (1.84 kW).

the other parameters at their optimised values as determined in the previous step. The results of this analysis are shown in figure 13. The flow-exit void model is significantly affected by heater/coolant interaction and gives an optimum $f_{ht} = 0.038$. The flow-pressure drop model, however, is not affected by heater/coolant interaction, since its minimum occurs at $f_{ht} = 0$.

5.3 *Optimised steady state results*

The experimental exit void fraction and pressure drop results are compared with the theoretical model results in figure 14. The agreement is generally satisfactory, particularly at the higher power levels. However, it could be noted that if the friction multiplier coefficient is assumed to be independent of power input, the model underestimates the pressure drop at the lower power levels, as shown in figure 11. The pressure drop data presented by Deev *et al.* (1978) and the more complicated forms of [18] derived by Beattie (1973) imply dependence of the multiplier coefficient on power input. In this investigation, this dependence has been assumed to be a linear function of the optimised parameter values at 1.70 and 1.84 kW.

A further measurement with which to validate the optimised mathematical model is the void transit times at the channel exit. The measured values are given by the maxima in the cross-correlation functions between the two void gauge signals, which were bandpass filtered in the frequency range 5–10 Hz to elucidate void propagation effects, and are shown in figure 15. The theoretical values are calculated from the ratio of the probe separation (45 mm) to the

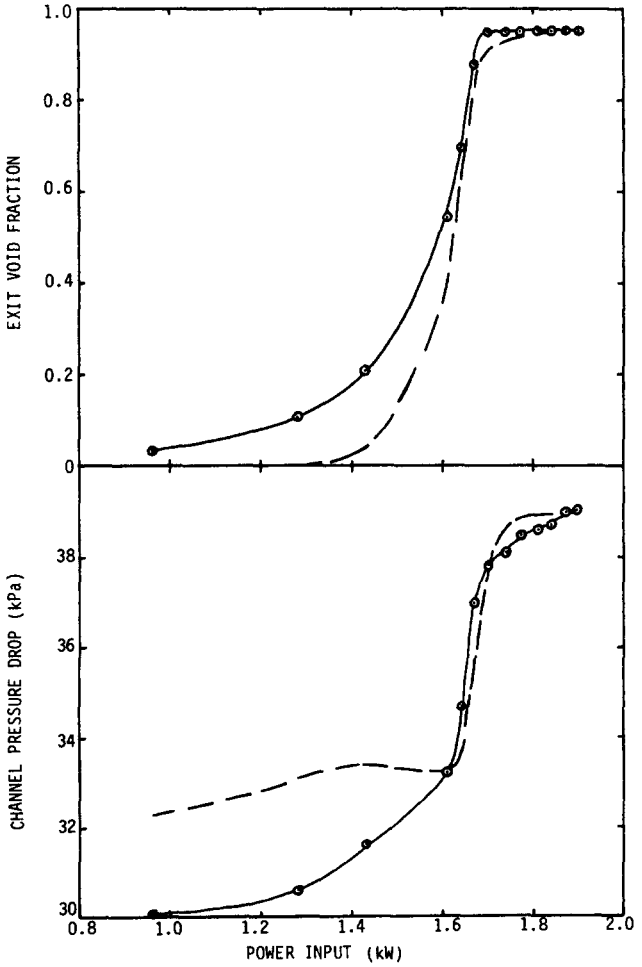

Figure 14. Comparison of experimental and theoretical steady state results with optimised coefficients (—⊙—experimental: --- theoretical).

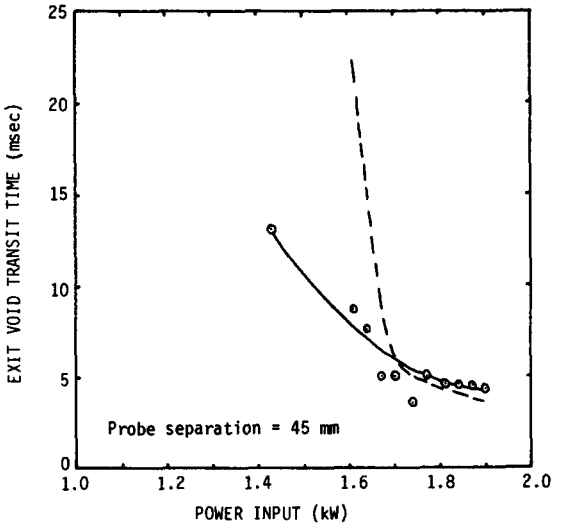

Figure 15. Vapour transit time between void probes at the channel exit (-⊙-, experimental: ---, theoretical, with slip).

channel exit vapour velocity. It can be seen that the agreement is good at the higher power levels, but poorer at the lower power levels where the errors between the measured and calculated steady state exit void fraction are greater.

5.4 *Optimised spectral results*

The cross-spectral density estimates of the flow-exit void and flow-pressure drop noise models at 1.84 kW are compared with their optimised theoretical model results in figure 16. The flow noise power spectral density estimates, which are used to perturb the theoretical model, have been weighted by their respective ordinary coherence estimates to account for extraneous noise sources on the input, as noted in section 5.2. The modulus results are in excellent agreement, particularly those for the flow-exit void model. The double peak in the theoretical flow-pressure drop modulus is due to the shape of its transfer function $\tilde{H}(\Delta p, w)$, which has a valley near the resonant frequency (Romberg 1978a).

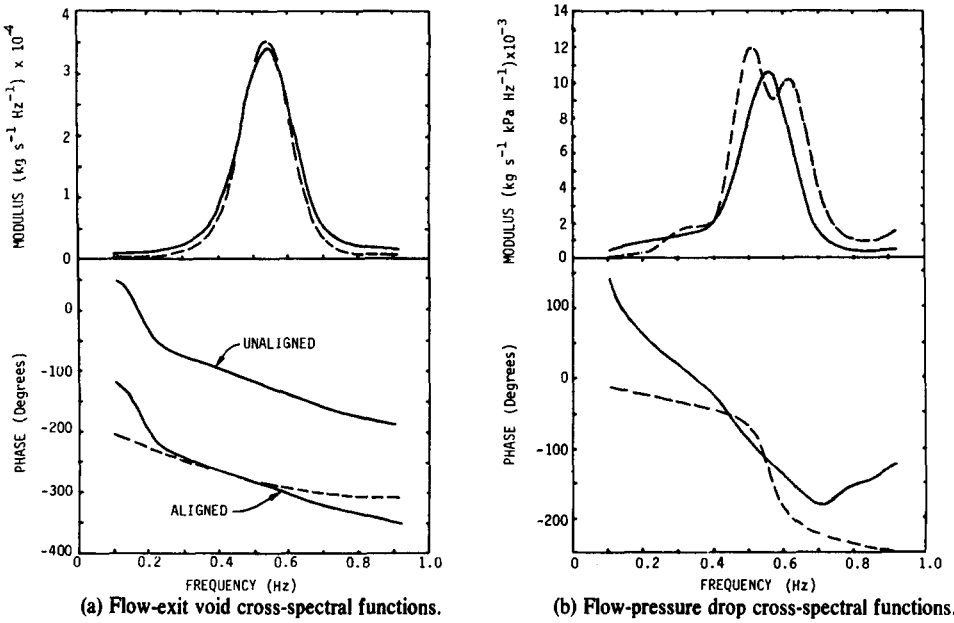

(a) Flow-exit void cross-spectral functions. (b) Flow-pressure drop cross-spectral functions.

Figure 16. Comparison of cross-spectral functions for the spectral and theoretical models (1.84 kW) (—— spectral: ---- theoretical).

As outlined in section 2.4 and figure 3, the phase results of the optimised theoretical model now become the reference for assessment of the noise model phase estimates. The errors in the flow-exit void phase estimates, when plotted as a function of frequency, were almost constant with a mean error of 165°. If this error, which is possibly caused by the different filters used in the flow and void measurements (figure 4), is subtracted from the phase estimates, the phase results are in excellent agreement, particularly in the frequency range of high coherence (0.4–0.6 Hz, figure 8a). The flow-pressure drop phase estimates are also compatible with the theoretical results in the frequency range of high coherence (figure 9a), but are in poorer agreement in the end range frequencies, where the coherence is low. (Note, the tolerance on the phase estimates is a function of the coherence estimates, Jenkins and Watts 1968.)

5.5 *Stability analysis*

The primary benefit of the optimised theoretical model is that it may be confidently used to assess the mechanisms which tend to drive the channel unstable. This information is given by the vector diagram of the transfer function components shown in figure 17, where vectors in the left half plane are destabilising, and vectors in the right half plane are stabilising. The vector for the total channel (T) lies in the left half plane, and therefore the channel is unstable. The dominant destabilising component is the two-phase momentum, which is mainly caused by the

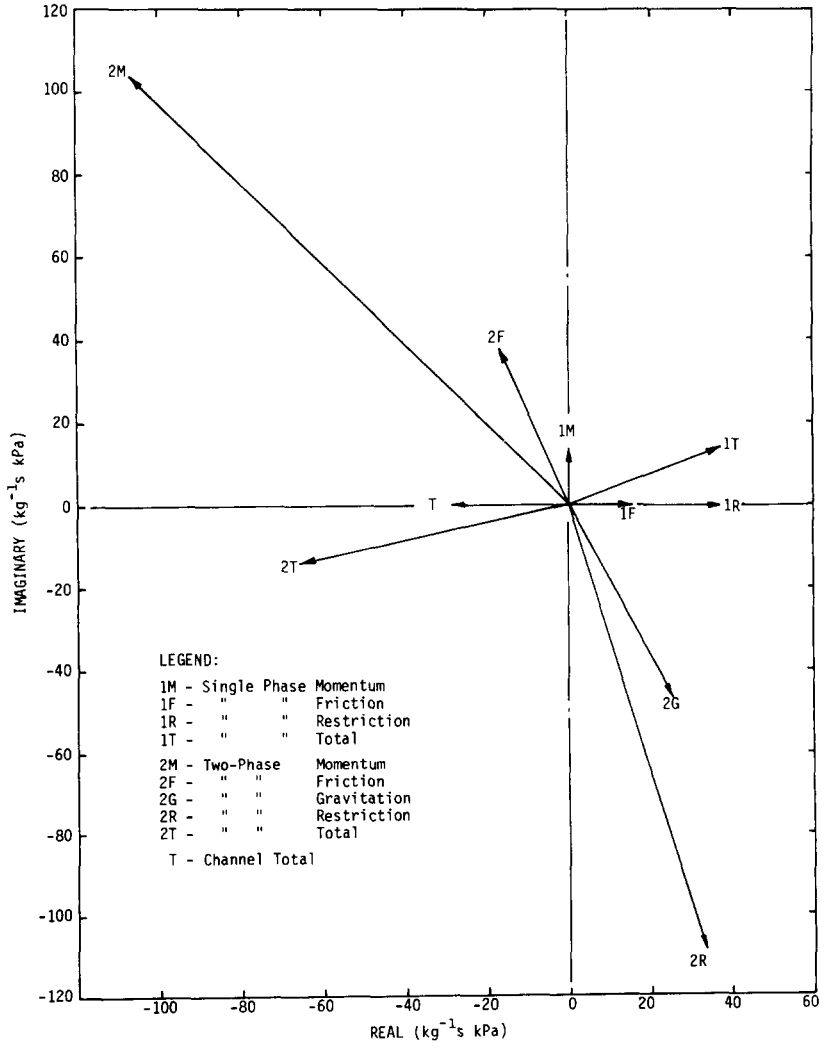

Figure 17. Vector diagram of transfer function components (1.84 kW) (crossover frequency = 0.595 Hz).

low pressure operating condition. The crossover frequency of 0.595 Hz agrees favourably with the channel resonant frequency (0.56 Hz). It could be noted that these model calculations do not include the effects of the riser (Appendix 1), which were negligible (Romberg 1978a).

6. CONCLUSIONS

The results presented in this paper have demonstrated that the hydrodynamic behaviour of boiling channels near the flow stability threshold may be assessed in relative detail by comparison of the dominant input–output cross-spectral functions of noise models based on inherent noise measurements with those calculated by a distributed theoretical model.

The main conclusions of this investigation are:

(1) The inverse variance of the flow noise monitored at the channel inlet is a linear function of the channel power prior to the onset of flow oscillations, and gives a reliable prediction of the instability threshold power (ITP). However, care must be exercised in computing the variance estimates if it is to be used as a reliable tool for diagnostic and control applications in commercial heat transfer systems.

(2) Multivariate spectral analysis of the noise measurements near the ITP proved that the flow-exit void and flow-pressure drop relationships are the most predominant in characterising system behaviour, i.e. the multivariate noise models are reducible to simpler bivariate models. However, some heat transfer systems (e.g. boiling water reactors with strong void coefficients of reactivity) may have more significant inlet temperature and power fluctuations than those monitored in the present test system, and should be analysed by multivariate modelling techniques.

(3) The flow-pressure drop relationship is the most sensitive indicator of the channel stability, and confirms that the channel behaviour near the ITP is best assessed from its hydraulic impedance characteristics, as has been hitherto assumed by most theoretical analyses.

(4) The optimised theoretical model results indicate that (a) the incipience of subcooled boiling is best predicted by the Nusselt number based on the equivalent heated diameter, (b) the voids were concentrated near the heater surface, and (c) the pressure drop measurements were influenced by a possible drag reduction mechanism, and is able to give a more realistic insight into the mechanisms tending to drive the channel unstable.

In summary, it has been shown how the inherent noise generated in a boiling channel may be used to obtain a relatively detailed understanding of its hydrodynamic behaviour. This "listening" technique presumes that the hydrodynamic/turbulent noise (or signal/noise) ratio is sufficiently high to ensure the reliability (coherence) of the relationships between the measured variables. The analyses need only be performed when an on-line surveillance strategy using the flow noise inverse variance or multivariate noise analysis (Piety & Robinson 1976) has detected the presence of significant hydrodynamic noise. It is the authors' view that the extensive range of flow stability investigations reported in the literature indicates that it is a recurring problem, particularly in systems with high power densities and/or complex designs, and demonstrates that further investigations of the inherent noise methods as outlined in this paper are warranted. The methods are sufficiently general, of course, to be used in hydrodynamic studies which use external pseudo-random perturbations instead of the inherent noise inputs.

Acknowledgements—The authors gratefully acknowledge the technical contributions of Mr. M. J. Hincksman, who assisted with the experiments and data analysis, and Mr. G. W. Herfurth, who assisted with the development of the void gauges. The helpful discussions and assistance given by Dr. R. W. Harris, Head, Applied Mechanics Section, A.A.E.C., are also gratefully acknowledged.

NOMENCLATURE

a coefficient, [18]
b coefficient, [18]
$\hat{C}_{ij}(f)$ co-spectral density estimate between ith and jth variables, Hz^{-1}
C_o distribution parameter
C_p specific heat
c coefficient, [18]
$F(z, t)$ arbitrary variable
f frequency, Hz
f_{ht} heat transfer factor, [19]
G mass flux, $kg\,s^{-1}\,m^{-2}$
g gravitational acceleration, $m\,s^{-2}$
$\hat{H}_{ij}(f)$ transfer function estimate between ith and jth variables
$\tilde{H}(y, x)$ transfer function between input (x) and output (y)
h specific enthalpy, $J\,kg^{-1}$
h_t heat transfer coefficient, $W\,m^{-2}{}^{\circ}C^{-1}$
K_f friction loss factor
K_o Bankoff factor
Nu Nusselt number
Pe Peclet number
$\hat{p}_{jN:M-1}(f)$ partial cross-spectral density estimate, Hz^{-1}
p pressure, kPa
Q power density, $W\,m^{-3}$
$\hat{Q}_{ij}(f)$ quad-spectral density estimate between ith and jth variables, Hz^{-1}
q heat flux, $W\,m^{-2}$
$R_{ij}(\tau)$ cross-correlation function between ith and jth variables
$\hat{S}_{ij}(f)$ cross-spectral density estimate between ith and jth variables, Hz^{-1}
St Stanton number
s Laplace operator
U velocity,$m\,s^{-1}$
V weighted mean vapour drift velocity, $m\,s^{-1}$
$w(\tau)$ lag window function
z axial distance, m
α void fraction
Δp pressure drop, kPa
ΔU_g vapour drift velocity, $m\,s^{-1}$
$\hat{\gamma}^2_{ij}(f)$ coherence estimate between ith and jth variables
θ angle of inclination to vertical
θ_T thermal capacitance per unit area, $J\,m^{-2}\,K^{-1}$
ρ density, $kg\,m^{-3}$
τ lag, s
τ_H heater time constant, s
ϕ^2 two-phase friction multiplier
$\hat{\psi}_{ij}(f)$ phase estimate between ith and jth variables

Subscripts

f saturated liquid, friction component
g saturated vapour
l subcooled liquid
o onset of subcooled boiling, fundamental mode
s source
w wall

Superscripts

$\hat{}$ estimate

$\tilde{}$ frequency dependent

REFERENCES

ANDERSON, T. T. 1970 Hydraulic impedance: a tool for predicting boiling loop stability. *Nucl. Appl. & Tech.* **9**, 422–433.

BEATTIE, D. R. H. 1971 Two-phase pressure losses flow regime effects and associated phenomena. Australian Atomic Energy Commission Rep. AAEC/TM 589.

BEATTIE, D. R. H. 1973 A note on the calculation of two-phase pressure losses. *Nucl. Engng & Design* **25**, 395–402.

BEATTIE, D. R. H. 1977 Some aspects of two-phase flow drag reduction. *2nd Int. Conf. Drag Reduction*, St. John's College, Cambridge, 31 Aug.–2 Sept., Paper D1.

BENDAT, J. S. & PIERSOL, A. G. 1971 *Random Data: Analysis and Measurement Procedures.* Wiley, New York.

BERGLES, A. E. 1972 Thermal-hydraulic instability—most recent assessments. *Proc. Symp. Two-phase Fluid Thermodynamics*, Rome, 9 June.

BJORLO, T., EUROLA, T., GRUMBACH, R., HANSSON, P., OLSEN, A., RASMUSSEN, J & ROMSLO, K. 1967 Comparative studies of mathematical hydrodynamic models applied to selected boiling channel experiments. EUR-4288e (1), pp. 981–1058.

BOURE, J. A., BERGLES, A. E. & TONG, L. S. 1973 Review of two-phase flow instability. *Nucl. Engng & Design* **25**, 165–192.

BOURÉ, J. A. 1975 On a unified presentation of the non-equilibrium two-phase flow models. CEA-CONF-3558.

BRIMLEY, W., NICOLL, W. B., STRONG, A. B. 1976 Flow oscillations in fixed-pressure-drop flow-boiling systems with random excitation. *Int. J. Heat Mass Transfer* **19**, 1379–1386.

CARVER, M. B. 1969 Effect of bypass characteristics on parallel-channel flow instabilities. *Proc. Inst. Mech. Engrs* **184**, 84–92.

DAVIES, A. L. & POTTER, R. 1967 Hydraulic stability: an analysis of the causes of unstable flow in parallel channels. *Symp. Two-Phase Flow Dynamics*, Eindhoven, EUR-4288e (2), pp. 1225–1266.

DAVIS, E. J. & DAVID, M. M. 1964 Two-phase gas–liquid convection heat transfer. *Ind. Engng Fundament.* **3**(2), 111–118.

DEEV, V. I., GORDEEV, Y. V., PRIDANTSEV, A. I., PETROVICHEV, V. I. & ARKHIPOV, V. V. 1978 Pressure drop in a two-phase flow of helium under adiabatic conditions and with heat supply. *Proc. 6th Int. Heat Transfer Conf.*, Montreal, 7–11 August, Vol. 1, pp. 311–314.

EUROLA, T. 1963 Reactor noise experiments on Halden boiling water reactor. *Noise Analysis in Nuclear Systems*, USAEC Rep. TID-7679, pp. 449–468.

EYKHOFF, P. 1974 *System Identification.* Wiley, New York.

FUKUNISHI, K. & KIYOKAWA, K. 1976 Dynamical analysis of a boiling water reactor by multivariable autoregressive model. *J. Nucl. Science & Technol.* **13**, 139–140.

FUKUNISHI, K. 1977 Coherence analysis of boiling water reactor noise. *J. Nucl. Sci. & Technol.* **14**(5), 351–358.

GALL, C. J. 1973 Assessment of the system response characteristics from 'noise' measurements at a single point with particular application to flow stability. *J. Br. Nucl. Energy Soc.* **12**, 175–181.

GRUMBACH, R. 1969 A systematic comparison of different hydrodynamic models. *Nucl. Sci. & Engng* **36**, 429–433.

JENKINS, G. M. & WATTS, D. G. 1968 *Spectral Analysis and its Applications.* Holden-Day, San Francisco.

JONES, A. B. 1961 Hydrodynamic stability of a boiling channel. USAEC Rep. KAPL-2170.

KROEGER, P. G. & ZUBER, N. 1968 An analysis of the effects of various parameters on the average void fractions in subcooled boiling. *Int. J. Heat Mass Transfer* **11**, 211–233.

NEAL, L. G. & ZIVI, S. M. 1965 Hydrodynamic stability of natural circulation boiling systems: a comparative study of analytical models and experimental data. TRW Rep. STL 372-14(1).

PIETY, K. R. & ROBINSON, J. C. 1976 An on-line reactor surveillance algorithm based on multivariate analysis of noise. *Nucl. Sci. & Engng* **59**, 369–380.

PRIESTLEY, M. B. 1969 Estimation of transfer functions in closed loop. *Automatica* **5**, 623–632.

RAKOPOULOS, C. D., EL-SHIRBINI, A. A. & MURGATROYD, W. 1978 An experimental investigation into the dynamics of two-phase flow in vapour generators. *Proc. 6th Int. Heat Transfer Conf.*, Montreal, 7–11 August, Vol. 1, pp. 357–362.

ROMBERG, T. M. & REES, N. W. 1975 Identification of a boiling channel and comparisons with a theoretical model for coolant flow stability analysis. *Proc. 6th IFAC Triennial World Cong.*, Boston.

ROMBERG, T. M. 1978a Noise analysis of coolant dynamics in boiling two-phase flow systems. Ph.D. Thesis, University of NSW.

ROMBERG, T. M. 1978b An algorithm for the multivariate spectral analysis of linear systems. *J. Sound & Vib.* **59**, 395–404.

ROMBERG, T. M. 1978c A note on the spectral analysis of linear systems with multiple inputs and outputs. *J. Sound & Vib.* **60**(1), 149–150.

SAHA, P. & ZUBER, N. 1974 Point of net vapor generation and vapor void fraction in subcooled boiling. *Proc. 5th Int. Heat Trans. Conf.*, Tokyo, Vol. IV, pp. 175–179.

SEINFELD, J. H. & LAPIDUS, L. 1974 *Mathematical Methods in Chemical Engineering: Process Modeling Estimation, and Identification* (Vol. 3). Prentice-Hall, New Jersey.

SPIGT, C. L. 1966 On the hydraulic characteristics of a boiling water channel with natural circulation. EURATOM Rep. Eur-2842e.

SPINKS, N. 1971 Analysis of flow stability in boiling systems with the TOSCLE code. Australian Atomic Energy Commission Rep. AAEC/E217.

TAKAHASHI R. & SHINDO, M. 1971 Theoretical study of two-phase flow oscillation in a hot channel—I. Theoretical study for interpreting the mechanism of hydrodynamic instability. *J. Nucl. Sci. & Tech.* **8**, 637–643; II. Influence of heat transfer characteristics on the flow stability. *J. Nucl. Sci. & Tech.* **8**, 690–695.

UHRIG, R. E. 1970 *Random Noise Techniques in Nuclear Reactor Systems.* Ronald Press, New York.

YADIGAROGLU, G. & BERGLES, A. E. 1972 Fundamental and higher-mode density-wave oscillations in two-phase flow. *J. Heat Transfer* **94**, 189–195.

ZUBER, N. & FINDLAY, J. A. 1965 Average volumetric concentration in two-phase flow systems. *J. Heat Transfer* **87**, 453–468.

ZUBER, N., STAUB, F. W., BIJWAARD, G. & KROEGER, P. G. 1967 Steady state and transient void fraction in two-phase flow systems. GEAP-5417.

APPENDIX 1

Test channel dimensions

REGION	LENGTH (cm)	DIAMETER (cm)	FLOW AREA (cm^2)	HYDRAULIC DIAMETER (cm)	
Inlet*	52.7	2.58 ID	5.238	2.58	Horizontal pipe with venturi flowmeter 45 dia. from inlet.
	17.8	0.953 ID 1.352 OD	0.722	0.399	Vertical annulus with T-junction at inlet.
Channel*	91.5	0.953 ID 1.352 OD	0.722	0.399	Vertical annulus with heated inner wall, glass outer wall.
Riser	91.5	2.54 ID	5.067	2.54	Vertical glass tube.

* Test region for input-output measurements = inlet + channel regions

APPENDIX 2

Experimental steady state results

HEATER POWER (kW)		INLET TEMP. (°C)		MASS FLOW (kg/s)		PRESSURE DROP (kPa)		EXIT VOID FRACTION		FLOW NOISE INVERSE VARIANCE	
Mean	Stan.Dev.	Mean	Stan.Dev.	Mean	Stan.Dev.	Mean	Stan.Dev.	Mean	Stan.Dev.	Mean	Stan.Dev.
0.964	± 0.002	35.32	± 0.79	0.135	±0.002	30.05	± 0.11	0.035	± 0.010	25.92	± 1.25
1.281	± 0.005	36.82	± 0.74	0.140	±0.004	30.62	± 0.11	0.105	± 0.007	26.53	± 1.48
1.433	± 0.010	37.91	± 0.82	0.142	±0.003	31.65	± 0.15	0.210	± 0.004	18.58	± 0.69
1.606	± 0.006	39.30	± 0.77	0.135	±0.003	33.18	± 0.19	0.546	± 0.008	10.19	± 0.33
1.637	± 0.007	40.07	± 0.77	0.126	±0.004	34.67	± 0.25	0.700	± 0.014	12.89	± 0.61
1.667	± 0.003	40.49	± 0.74	0.108	±0.004	36.99	± 0.36	0.880	± 0.006	11.27	± 0.46
1.701	± 0.003	40.85	± 0.13	0.096	±0.003	37.84	± 0.12	0.947	± 0.006	9.54	± 0.45
1.736	± 0.004	41.01	± 0.13	0.093	±0.004	38.11	± 0.26	0.954	± 0.008	8.45	± 0.23
1.765	± 0.005	41.12	± 0.00	0.091	±0.004	38.45	± 0.11	0.954	± 0.004	6.90	± 0.25
1.809	± 0.007	41.28	± 0.12	0.0890	±0.005	38.60	± 0.09	0.952	± 0.004	6.04	± 0.27
1.835	± 0.008	41.38	± 0.12	0.0883	±0.005	38.71	± 0.13	0.951	± 0.003	3.78	± 0.18
1.867	± 0.004	41.69	± 0.16	0.0931	±0.006	38.96	± 0.19	0.952	± 0.008	4.73	± 1.42
1.899	± 0.004	41.76	± 0.12	0.0966	±0.012	39.01	± 0.33	0.954	± 0.013	1.39	± 0.52

APPENDIX 3

Parameter limits for two-phase correlations

CORRELATION	EQUATIONS	PARAMETER LIMITS	REFERENCE	REMARKS
Subcooled Boiling Boundary	(12)	1) Nu=455, St=0.0065 2) Nu=188, St=0.0027	Saha & Zuber (1974)	1) Based on equivalent hydraulic diameter 2) Based on equivalent heated diameter
Two-phase Slip	(16),(17)	1) C_o = 1.0, V = 0 2) C_o = 1.2, V = 0	- Zuber et al (1967)	1) Homogeneous flow (no slip) 2) Bubbly flow, no drift
Two-phase Friction	(18)	1) a=1, b=1, c=0 2) a=1.368, b=1, c=0	- Beattie (1971)	1) Homogeneous flow 2) Bubble flow, $a \approx (3.5)^{0.25}$